8-12-2003

Mechanical properties of magnetostrictive iron-gallium alloys

R. A. Kellogg
Iowa State University

Alan M. Russell
Iowa State University, russell@iastate.edu

Thomas A. Lograsso
Iowa State University, lograsso@ameslab.gov

A. B. Flatau
University of Maryland - College Park

A. E. Clark
Clark Associates

See next page for additional authors

Mechanical properties of magnetostrictive iron-gallium alloys

R.A. Kellogg,[a*] A.M. Russell,[b,c] T.A. Lograsso,[b,c] A.B. Flatau,[d] A.E. Clark,[e] and M. Wun-Fogle[f]

[a] Aerospace Engineering and Engineering Mechanics Department,
[b] Department of Materials Science and Engineering,
[c] Ames Laboratory of the U.S. Department of Energy,
Iowa State University, Ames, IA, USA
[d] Aerospace Engineering Department, University of Maryland, 20742, MD, USA
[e] Clark Associates, Adelphi, MD 20783
[f] Naval Surface Warfare Center, Carderock Division, Code 645, W. Bethesda, MD 20817

ABSTRACT

Single crystal specimens of Fe-17 at. % Ga were tested in tension at room temperature. Specimens with a tensile axis orientation of [110] displayed slip lines on the specimen faces corresponding to slip on the {110}<111> with a critical resolved shear stress τ_{CRSS} = 220 MPa. Yielding began at 0.3% elongation and 450 MPa. An ultimate tensile strength of 580 MPa was observed with no fracture occurring through 1.6% elongation. The Young's modulus was 160 GPa in the loading direction with a Poisson's ratio of -0.37 on the (100) major face. A specimen with a tensile axis orientation of [100] showed slip lines corresponding to slip on the {211}<111> with τ_{CRSS} = 240 MPa. Discontinuous yielding began at 0.8% elongation, which was thought to result from twinning, kink band formation, or stress-induced transformation. The Young's modulus was 65 GPa in the loading direction with a Poisson's ratio of 0.45 on the (001) major face. A maximum tensile strength of 515 MPa was observed with fracture occurring after 2% elongation. A sizeable elastic anisotropy of 19.9 was identified for Fe-27.2 at. % Ga accompanied by a Poisson's ratio of -0.75 to produce a large in-plane auxetic behavior.

Keywords: Galfenol, magnetostrictive, iron, gallium, mechanical properties, negative Poisson's ratio, auxetic

1. INTRODUCTION

Alloys of iron substituted with non-magnetic gallium exhibit coupling between their mechanical and magnetic states and offer promise as mechanically robust actuator/sensing materials.[1] Studies of single crystal $Fe_{100-x}Ga_x$, where $13 \le x \le 23$, have shown the alloys to undergo magnetostrictive strains approaching 400 ppm with low saturating fields of several hundred oersteds as well as displaying a limited temperature dependence over a -20 to 80°C range.[2, 3, 4] The possible challenges in shaping this material to produce engineering components and the need to impart a preferred crystallographic texture to optimize the magnetostrictive performance of polycrystalline forms motivated this study of the alloy's mechanical properties. To determine the alloy's active slip systems, critical resolved shear stresses, elastic moduli, and Poisson's ratios we examined the single crystal response to tensile loading. Ga exhibits extensive solid solubility in body-centered cubic (BCC) α-Fe. The 17 at. % Ga content of the alloy used in this study is a single-phase solid solution from room temperature to 1673 K with Ga atoms randomly substituted throughout the lattice structure. The curie temperature is 973 K.

Polycrystalline metals are often isotropic due to their overall random crystallographic distribution, however single crystal and strongly textured polycrystalline BCC metals exhibit a high degree of anisotropy in their mechanical characteristics. Miller indices are used to identify a specimen's crystallographic orientation and the directionally dependent elastic and plastic responses arising from a given state of mechanical loading. Grouped Miller indices of a particular fiber direction and families of equivalent fiber directions are represented as the vectors [*u v w*] and <*u v w*>, respectively. Similarly, a plane surface is denoted by the notation (*k h l*) with indices representing the plane-normal vector. The family of equivalent planes is given as {*h k l*}. Representative of a Fe-Ga alloy, Fig. 1 shows a schematic of the BCC structure with several fiber directions and a plane highlighted as examples of the Miller indices notation.

*Corresponding author: 2271 Howe Hall, room 1200; ph: (515) 294-0088; e-mail: rkellogg@iastate.edu

The positive Cartesian axes represent three of six possible vectors from the <100> fiber group. The highlighted $[11\bar{1}]$ fiber lies within the (101) plane and is one of the eight-member <111> fiber group. The (101) plane is one of eight belonging to the {110} family of planes.

The mechanical properties of a BCC crystal lattice are inherently anisotropic due a directional dependence in the atomic packing density (Fig. 1). As an example of anisotropic plastic deformation, we consider the slip mechanisms in high purity (99.96%) α-Fe. At room temperature the primary slip system is {110}<111> with slip occurring at a critical resolved shear stress (τ_{CRSS}) of 27.5 MPa.[5] The {110} set of planes is favored for slip as they are the planes of highest planar atomic packing density, thus presenting the lowest energy barrier to dislocation movement. Similarly the <111> family of slip directions are favored as they possess the highest linear atomic packing density within the {110} planes. Inhibited by lower relative atomic packing densities, secondary slip occurs in pure α-Fe on the {211}<111> and {321}<111>.

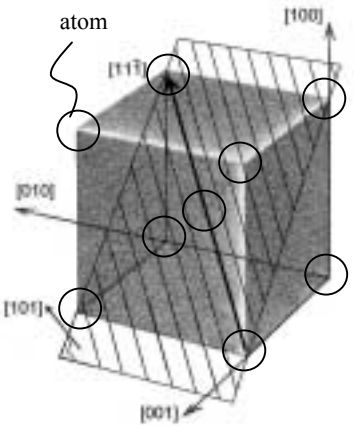

Fig. 1. Schematic of BCC crystal with the (101) plane, and $[11\bar{1}]$ and <100> fiber directions highlighted.

The elastic response of BCC crystals to loading is also directionally dependent. For example, the Young's modulus E in single crystal α-Fe exhibits its lowest value in the direction of lowest atomic packing density. In this case $E_{[100]}$ = 131 GPa, where the subscript indicates the direction of measurement. An intermediate modulus occurs in the [110] direction where $E_{[110]}$ = 219 GPa. Accordingly, the maximum observed modulus value is $E_{[111]}$ = 283 GPa in the [111] direction, which is the direction of highest atomic packing density[6].

The analysis of a material's anisotropic elastic properties is facilitated using the generalized Hook's law (Eq.1). In the case of cubic crystals, symmetry permits the relationships between stress σ_i and strain e_j to be completely defined using the three second-order engineering elastic constants c_{11}, c_{12} and c_{44}.[7]

$$\sigma_i = c_{ij} e_j \qquad \text{where} \quad i = 1, 2, \ldots 6;\ j = 1,2, \ldots 6, \tag{1}$$

and $c_{11} = c_{22} = c_{33}$; $c_{12} = c_{21} = c_{13} = c_{31} = c_{32} = c_{23}$; $c_{44} = c_{55} = c_{66}$. All other c_{ij} = 0. Utilizing rotational coordinate transformations for stress and strain, the elastic properties such as Young's modulus and Poisson's ratio may be stated in terms of c_{ij} for any direction[8]. Just as the Young's modulus was anisotropic so is the Poisson's ratio. The Poisson's ratio $\nu_{[uvw]}$ is defined as the negative ratio of transverse strain to longitudinal strain that results from loading in the longitudinal direction. The *[uvw]* subscript indicates the direction of the transverse strain measurement.

The anisotropy of a cubic material's elastic properties may be emphasized by analyzing the elastic relationships of two high-symmetry crystal orientations and loading directions that generate minimum or maximum crystal lattice shear stress conditions. The effects of c_{11} and c_{12} may be expressed independently from c_{44} through uniaxial [100] loading of a (001)[100] single crystal. With this loading condition the directionally dependent relationships for E and ν arise as given in Eqs. 2 and 3.[9]

Young's modulus:
$$E_{[100]} = \frac{c_{11} R}{c_{11} + c_{12}} \tag{2}$$

Poisson's ratios:
$$\nu_{[010]} = \nu_{[001]} = \frac{c_{12}}{c_{11} + c_{12}}, \tag{3}$$

where
$$R = \frac{1}{c_{11}} (c_{11} - c_{12})(c_{11} + 2c_{12}).$$

The effect of c_{44} on the elastic response becomes definitive for the uniaxial [110] loading of a (001)[110] single crystal. If the values of c_{11} and c_{12} are known, c_{44} may be easily related to the directionally dependent values of E and ν given in Eqs. 4, 5, and 6 where R is the same as used above.[9]

Young's modulus: $$E_{[110]} = \frac{4c_{44}R}{R+2c_{44}} \quad (4)$$

The first Poisson's ratio: $$\nu_{[1\bar{1}0]} = \frac{R-2c_{44}}{R+2c_{44}}, \quad (5)$$

The second Poisson's ratio: $$\nu_{[001]} = \frac{4c_{12}c_{44}}{c_{11}(R+2c_{44})}, \quad (6)$$

Depending on the values of c_{11}, c_{12} and c_{44}, the Poisson's ratios $\nu_{[1\bar{1}0]}$ and $\nu_{[001]}$ may be dramatically different. Remarkably, many BCC and FCC systems exhibit negative values of $\nu_{[1\bar{1}0]}$ while $\nu_{[001]}$ is always positive.[9, 10] The negative Poisson's ratio described here is a two-dimensional effect. When $\nu_{[1\bar{1}0]}$ is negative, as a consequence of approximate volume conservation, $\nu_{[001]}$ is correspondingly large and positive in the third dimension. Negative Poisson's materials are known as possessing "auxetic" behavior and for the case of the in-plane negative Poisson's ratio described by Eq. 5, the phenomena is termed "in-plane auxetic" behavior. Jain *et al*. has shown that the anisotropy parameter "*A*" (Eq. 7) is a convenient measure of a material's propensity for exhibiting in-plane auxetic behavior.[9]

$$A = \frac{2c_{44}}{c_{11}-c_{12}} \quad (7)$$

Metallic crystals generally have values of $A > 1$. It has been shown that $\nu_{[1\bar{1}0]}$ must be positive for $A < 2$, that $\nu_{[1\bar{1}0]}$ may be positive or negative when $2 < A < 3$, and that $\nu_{[1\bar{1}0]}$ must be negative if $A > 3$. In the limit of $c_{11} - c_{12} = 0$, A approaches infinity and $\nu_{[1\bar{1}0]}$ approaches its minimum value of -1.0.[9]

To provide a point of reference, the elastic constants of high purity α-Fe are c_{11} = 228 GPa, c_{12} = 132, c_{44} = 116.5.[6] These values give the directionally dependent Young's moduli of $E_{[100]}$ = 131 and $E_{[110]}$ = 219 GPa. The Poisson's ratios associated with these moduli are also anisotropic where [100] loading gives $\nu_{[010]} = \nu_{[001]} = 0.37$ and [110] loading gives $\nu_{[1\bar{1}0]}$ = -0.06 and $\nu_{[001]}$ = 0.61. Pure α-Fe exhibits a slight in-plane auxetic behavior which is consistent with the anisotropy parameter A = 2.4. In what follows, we examine this behavior in Fe-Ga alloys.

The Fe-Ga alloy specimen preparation and tensile testing procedures are discussed in section 2 followed by a report of the experimental results and analysis of plastic and elastic deformation in section 3. Section 4 discusses the plastic slip results and considers the crystallographic texture formation and environmental embrittlement observed in potentially similar alloy systems. In addition, the elastic properties of other Fe-Ga stoichiometries are reviewed to reveal trends in the elastic anisotropy and in-plane auxetic behavior.

2. EXPERIMENTAL PROCEDURES

2.1 Materials preparation

A single crystal of $Fe_{83}Ga_{17}$ was grown in an alumina crucible by the modified Bridgman technique. The starting ingot for single crystal growth was prepared by arc-melting appropriate quantities of Fe (99.99% purity) and Ga (99.999% purity) metal several times under an Ar atmosphere. The button was then remelted, and the alloy was drop cast into a Cu chill cast mold to ensure compositional homogeneity throughout the ingot.

The alloy was heated under a pressure of 1.3 x 10^{-4} Pa up to 1075 K to degas the crucible and charge. The chamber was then backfilled to a pressure of 275 kPa with high purity Ar. The ingot was then further heated to the growth temperature and held for 1 hour to allow thorough mixing before withdrawing the sample from the heat zone at a rate of 4 mm/h. Following growth, the ingot was annealed at 1000°C for 168 hours. X-ray diffraction analysis confirmed the crystal's single-phase, fully disordered α structure.

The single crystal's orientation was determined within 0.25° using Laue X-ray back reflection analysis and then cut into tensile specimens (Fig. 2) by electro-discharge machining. After machining, the orientation of each specimen was again checked by Laue X-ray back reflection analysis. The major and minor faces of the specimens' gauge length were

polished with progressively finer wetted silicon carbide paper to 800 grit and finished with 1 μm diamond paste in an oil suspension to provide a smooth surface for slip line observation.

2.2 Tensile testing procedures

Four single crystal tensile specimens of $Fe_{83}Ga_{17}$ were tested. Two were cut with the [110] direction parallel to the tensile axis. The major faces of these specimens were (001) planes, and the minor faces were $(1\bar{1}0)$ planes. The other two specimens were cut with the [100] direction parallel to the tensile axis. The major and minor faces of those specimens were {100} planes. Schematics of the two crystal orientations and their dimensioned geometries are shown in Fig. 2. The wedge-shaped ends facilitated gripping the specimen during tensile loading. Strain gages were attached on opposing major faces near the specimen midpoint to measure the longitudinal and transverse strains. The specimen surface under each strain gage was abraded prior to gage installation to improve bonding.

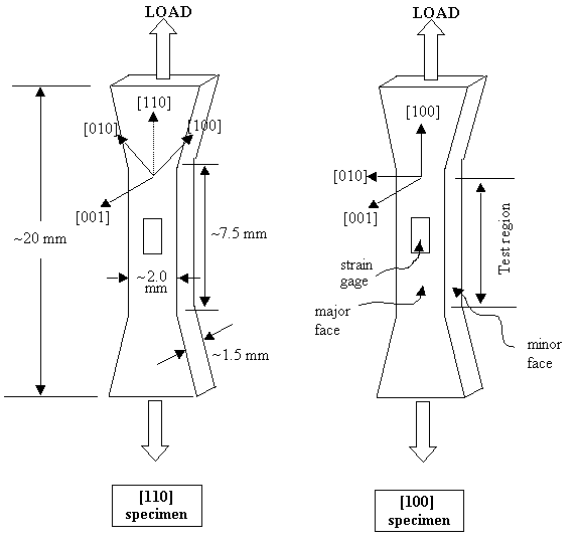

Fig. 2. Schematic of [110] and [100] oriented single crystal tensile specimen geometry with loading direction and strain gage locations indicated. Dimensions are approximately the same for all specimens.

Tensile tests were conducted at room temperature in air of normal humidity. Specimens were pulled using a hydraulic MTS machine with the cross arm operating in constant velocity mode at ~0.5 μm/s. During the course of each tensile test the loading changes on the MTS load frame and related fixturing led to slight changes in dimension of the overall test system. As a result, the specimens were subjected to a minor variation in strain rate. Over each specimen's elastic response regime the strain rate was ~3 x 10^{-6} s^{-1}. Over each specimen's plastic deformation regime the system load remained more constant and the constant cross arm velocity generated a strain rate of ~18 x 10^{-6} s^{-1}. The tensile test of each specimen took roughly 30 minutes from start to finish. The cross arm displacement, load, and longitudinal and transverse strain gage outputs were digitally recorded at 10 Hz. Specimens were pulled up to ~2% strain to develop distinct slip lines without excessive rotation of the original crystal lattice orientation. Slip lines were digitally photographed using both optical and scanning electron microscopy and their orientation with respect to the tensile axis was determined by computer aided image analysis.

3. EXPERIMENTAL RESULTS AND ANALYSIS

3.1 Tensile tests with [110] parallel to the tensile axis

The two single crystal tensile specimens of $Fe_{83}Ga_{17}$ oriented with the tensile axis parallel to the [110] direction displayed sufficient ductility to allow determination of the active slip system and the probable critical resolved shear stress τ_{CRSS}. The strain gage data for one of these specimens was collected to provide a stress-strain plot (Fig. 3). Analysis of the response gave $E_{[110]}$ = 160 GPa in the loading direction and $\nu_{[1\bar{1}0]}$ = -0.37 on the (001) major face. Yielding began at 450 MPa and 0.3% elongation leading to a projected 0.2% yield stress of 530 MPa. An ultimate tensile strength of 580 MPa was observed with no fracture occurring through 1.6% elongation. The test was terminated at 1.6% strain with the onset of decreasing tensile load.

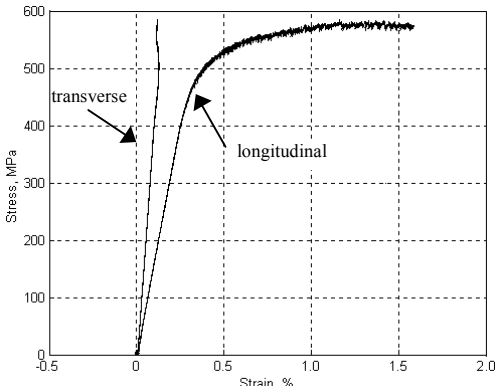

Fig. 3. Stress vs. strain plot for $Fe_{83}Ga_{17}$ single crystal tensile test with the tensile axis parallel to the [110] direction. Note that the positive transverse strain gives a negative Poisson's ratio.

As viewed in the optical microscope, the (001) major faces of the specimens displayed two sets of slip lines at a 47.3° angle with the tensile axis (Fig. 4a). The $(1\bar{1}0)$ planes of the minor faces showed two sets of slip lines, each of which forms a 35.0° angle with the tensile axis (Fig 4b).

Four slip planes were considered as candidates for slip in this alloy: {100}, {110}, {211}, and {321}. These four planes are the only planes in the BCC structure with a reasonably high planar atomic packing density, so they are usually considered to be the only plausible slip plane candidates in the BCC structure.[11] Fig. 1 shows a (101) plane as an example of the {110} group. The angles of slip lines for each of these candidate slip planes were calculated for both the major and minor faces of these specimens, and the results of these calculated angles were compared to the observed slip line angles from our tensile test specimens. The results of this comparison are shown in Table 1.

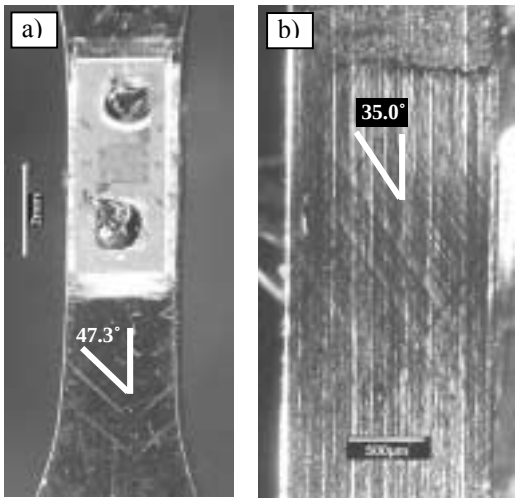

Fig. 4. Optical micrographs of $Fe_{83}Ga_{17}$ single crystal slip lines with its tensile axis parallel to the [110] direction. The angle of the slip lines with the tensile axis are indicated. a) The (100) major face of a tensile test specimen. b) The $(1\bar{1}0)$ minor face of a tensile test specimen.

Table 1. Calculated angles of slip lines for four candidate slip planes for a specimen with the tensile axis parallel to the crystallographic direction. The observed slip line angles are shown in the lower portion of the table for comparison. Note that only the {110} calculated slip plane angles are consistent with the observed slip line angles.

Slip Plane	Calculated Slip Line Angles with the Tensile Axis on the Major Face	Calculated Slip Line Angles with the Tensile Axis on the Minor Face
{100}	45˚, 90˚	0˚, 90˚
{110}	0˚, 45˚, 90˚	35.3˚, 90˚
{211}	0˚, 18.4˚, 71.6˚, 90˚	0˚, 35.3˚, 64.8˚
{321}	11.3˚, 18.4˚, 26.6˚, 63.4˚, 71.6˚, 78.7˚	13.3˚, 35.3˚, 54.7˚ 74.2˚

Observed Slip Line Angles with the Tensile Axis on the Major Face	Observed Slip Line Angles with the Tensile Axis on the Minor Face
47.3˚	35.0˚

Slip on the {110}, {211}, and {321} planes are all capable of producing slip lines on the minor face with an angle of 35.3˚ to the [110] direction of the tensile axis. However, only the {110} slip plane shows a reasonable match between the calculated and observed slip line angles on both the major and minor faces simultaneously. We attribute the 0.3˚ discrepancy between the observed angle of 35.0˚ and the calculated angle of 35.3˚ to errors in measurement (principally small deviations from a perpendicular viewing line of sight while photographing slip lines in the microscope) and to slip plane rotation during the 1.6% strain of the samples. The disparity between the calculated 45˚angle and the observed 47.3˚ angle is thought to have similar causes. From this analysis we conclude that the active slip plane in these specimens was the {110}.

There are three slip directions lying on the {110} planes that have a reasonably high linear atomic density in the α structure; these are <111>, <100>, and <110> (Table 2). Of these, the <111> is the most likely slip direction since it has substantially higher linear packing density than the others, and it is the dominant slip direction in BCC metals. Fig.1 shows the $[11\bar{1}]$ direction as an example. However, to test the feasibility of slip in the <100> and <110> directions, a Schmid factor analysis was performed.

Table 2. Schmid factors, $(\cos\phi)(\cos\gamma)$, and critical resolved shear stress for three possible slip directions on the {110} plane in a specimen with the tensile axis parallel to the [110] crystallographic direction. Note that all three directions have non-zero Schmid factors, so each direction is a possible slip direction on the {110} planes. As discussed in Section 3.1, the <111> direction is believed to be the most probable slip direction.

Slip Direction	Schmid factor for {110} Slip Plane with a [110] Tensile Axis	Critical resolved shear stress for {110} Slip Plane with a [110] Tensile Axis
<111>	0.41	220 MPa
<100>	0.35	190 MPa
<110>	0.25	130 MPa

Recalling Schmid's Law (Eq. 8) for resolved shear stress [5]:

$$\tau = \sigma(\cos\phi)(\cos\gamma) \quad (8)$$

where τ is the shear stress on a given slip plane, σ is the tensile stress on the sample, ϕ is the angle between the slip plane's normal vector and the tensile axis, and γ is the angle between the slip direction and the tensile axis. The $(\cos\phi)(\cos\gamma)$ product is often referred to as the Schmid factor. Orientations with a large Schmid factor (0.5 is the maximum value possible) are favored for slip since the shear stress (τ) needed to move dislocations is directly proportional to the Schmid factor for a given tensile stress (σ) on the crystal.

The <111> slip direction has a large Schmid factor in this test orientation (Table 2); the <100> and <110> directions have smaller, but non-zero Schmid factors. Thus, we conclude that it is probable that the slip direction was <111> in this specimen, but the possibility of slip in the <100> and <110> directions cannot be ruled out. If <111> is assumed to be the slip direction, the τ_{CRSS} = 220 MPa for slip on the {110}<111>.

3.2 Tensile tests with [100] parallel to the tensile axis

The single crystal tensile specimens of $Fe_{83}Ga_{17}$ oriented with the tensile axis parallel to the <100> direction also displayed sufficient ductility to allow determination of the active slip system and the probable τ_{CRSS}. The strain gage data for one of these specimens was collected to provide a stress-strain plot (Fig. 5). Analysis of the response gave $E_{[100]}$ = 65 GPa in the loading direction and $\nu_{[010]}$ = 0.45 on the (001) major face. Discontinuous yielding began at 0.8% elongation, which was thought to result from twinning, kink band formation, or stress-induced phase transformation. A clearly audible sound similar to that of twinning accompanied the discontinuous yielding event between 0.8 and 1.5% strain. Several more acoustic events occurred beyond 2% strain at progressively lower stress levels. A maximum tensile strength of 515 MPa was observed with fracture occurring shortly after 2% elongation. Strain gage data collection was terminated at -0.3% and 2.0% strains.

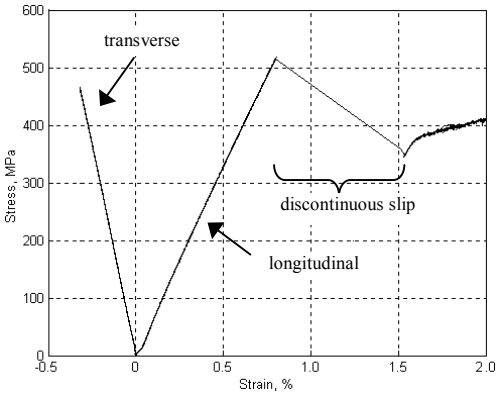

Fig. 5. Stress vs. strain plot for $Fe_{83}Ga_{17}$ single crystal tensile test with the tensile axis parallel to the [100] direction. Strain gage data collection was terminated at -0.3% and 2.0% strains.

As viewed in the optical microscope and the SEM, the {100} major faces and {100} minor faces of the specimens displayed two sets of slip lines at a 63.2˚ angle with the tensile axis (Fig. 6a and Fig. 6b).

As Table 3 indicates, both the {211} and {321} slip planes are consistent with the 63.2˚ angle observed on the major and minor specimen faces. It is possible, however, to discriminate which of these two planes is slipping by calculating the Schmid factors of all 24 {211} slip planes and all 48 {321} slip planes (assuming <111> slip directions). If the particular planes that form 63.4˚ slip lines are the same ones that have the largest Schmid factors for this tensile axis orientation, then slip may be occurring on that plane; however, if the particular planes that form 63.4˚ slip lines do not have the largest Schmid factors for this tensile axis orientation, then that slip plane cannot be the one that is active in these specimens. In the {321} family of planes, the specific planes that would form a 63.4˚ slip line on the major and minor

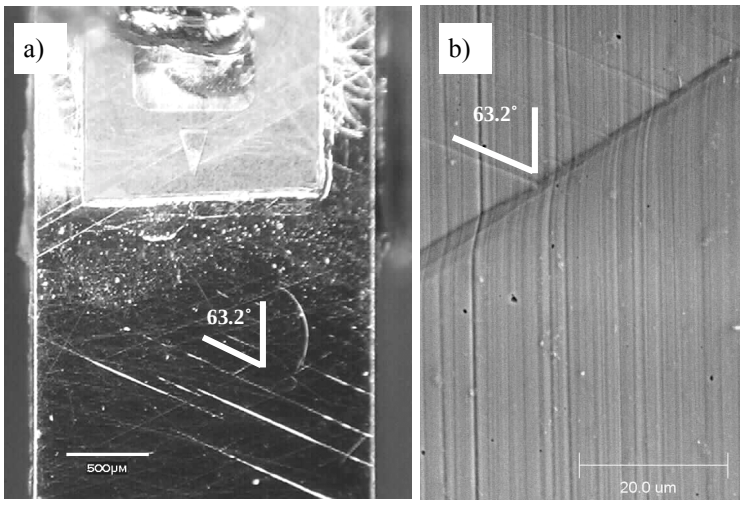

Fig. 6. Micrographs of slip lines of a $Fe_{83}Ga_{17}$ single crystal tensile test specimen with its tensile axis parallel to the [100] direction. The angle of the slip lines with the tensile axis are indicated. a) Optical micrograph of the (001) major face b) SEM of the (010) minor face. The prominent slip line from middle left to upper right is a possible twinned or kink band region. The vertical lines are polishing artifacts.

faces are the eight possible sign permutations of the (312) planes. Those eight planes all have a Schmid factor of 0.31. However, other {321} planes have a Schmid factor of 0.46, and those planes did not form slip lines on the specimen faces. This indicates that {321} slip did not occur in these specimens. In the case of the {211} planes, the planes that have the largest Schmid factor (0.47) are the eight sign permutations of the (211). All other {211} planes have smaller Schmid factors, which indicates that {211} slip is possible. Since no other candidate slip plane satisfies the slip criteria and the <111> direction lies in the slip plane with the largest Schmid factor, as shown in Table 4, we conclude that the slip observed in these specimens was {211}<111>.

Table 3. Calculated angles of slip lines for four candidate slip planes for a specimen with the tensile axis parallel to the [100] crystallographic direction. The observed slip line angles are shown in the lower portion of the table for comparison. Note that both the {211} and {321} calculated slip plane angles are consistent with the observed slip line angles.

Slip Plane	Calculated Slip Line Angles with the Tensile Axis on the Major and Minor Faces
{100}	90˚
{110}	45˚, 90˚
{211}	26.6˚, 45˚, 63.4˚
{321}	18.4˚, 26.6˚, 33.7˚, 56.3˚, 63.4˚, 71.6˚

Observed Slip Line Angle with the Tensile Axis on the Major and Minor Face
63.2˚

Determination of the yield stress in this specimen is problematical since, as Fig. 5 shows, a discontinuous yield event occurred before 0.2% offset strain was reached. For this reason, the 515 MPa stress value at the onset of the discontinuous yielding was used as the yield stress value. For the <111> slip direction (Table 4), a 515 MPa yield stress value can be used in Schmid's Law to estimate that $\tau_{CRSS} \approx$ 240 MPa for slip on the {211}<111>. This τ_{CRSS} is only slightly higher than the 220 MPa value determined for {110}<111> slip (Section 3.1). The highest Schmid factor for {110}<111> slip in the specimens with the [100] direction as the tensile axis is 0.41, which is lower than the 0.47 Schmid factor calculated for {211}<111> slip in these specimens. Thus, since the τ_{CRSS} values were nearly equal for these two slip systems, one would expect {211}<111> slip to occur in preference to {110}<111> slip, and indeed that was observed in these specimens.

Table 4. Schmid factors, $(\cos \phi)(\cos \gamma)$, and critical resolved shear stress for three slip directions on the {211} plane in a specimen with the tensile axis parallel to the [100] crystallographic direction.

Slip Direction	Schmid factor for {211} Slip Plane with a [100] Tensile Axis	Critical resolved shear stress for {211} Slip Plane with a [100] Tensile Axis
<111>	0.47	240 MPa
<110>	0.29	148 MPa
<100>	No <100> directions in the {211}plane	--------

3.3 Determination of elastic constants

The three elastic constants c_{11}, c_{12}, and c_{44} for the single crystal $Fe_{83}Ga_{17}$ alloy may be determined from the [100] and [110] oriented crystals' Young's moduli and Poisson's ratios. The simultaneous solution of Eqs. 2 and 3 allow constants c_{11} and c_{12} to be calculated (Eqs. 9 and 10) in terms of $E_{[100]}$ and $\nu_{[010]}$.

$$c_{11} = \frac{(1-\nu_{[010]})E_{[100]}}{(1+\nu_{[010]})(1-2\nu_{[010]})} \tag{9}$$

$$c_{12} = \frac{\nu_{[100]}E_{[100]}}{(1+\nu_{[010]})(1-2\nu_{[010]})} \tag{10}$$

Accounting for the maximum error in stress and strain, the variable $E_{[100]}$ is known to within 3% for this sample. The error in the Poisson's ratio is estimated at less than 1% by considering the combined error in longitudinal and transverse strain measurements. Using values of $E_{[100]} = 64.5 \pm 1.8$ GPa and $\nu_{[010]} = 0.445 \pm 0.004$ (from Fig. 3) then $c_{11} = 225 \pm 20$ GPa and $c_{12} = 181 \pm 20$ GPa. Notice that the difference in these elastic constants, c_{11}-$c_{12} = E_{[100]}/(1 + \nu_{[010]}) = 44.6 \pm 1.3$

GPa, has a relatively small error bar compared to either c_{11} or c_{12} alone. This fact suggests that the c_{44} and the anisotropy parameter A (Eq. 7) may be known with higher accuracy.

To estimate the value of c_{44}, either Eqs. 4, 5 or 6 may be used in conjunction with the previously determined values of c_{11} and c_{12}. Since both $E_{[110]}$ and $\nu_{[1\bar{1}0]}$ were measured in this study, comparisons of c_{44} calculated using Eqs. 4 and 5 are possible. The values of $E_{[110]}$ = 160.4 ± 1.8 GPa and $\nu_{[1\bar{1}0]}$ = -0.374 ± 0.004 were determined from the [110] specimen's stress-strain curves (Fig. 5) where the same range of error conditions were present as in the testing of the [100] oriented specimen. A sensitivity analysis shows that admissible solutions satisfying both Eqs. 4 and 5 give c_{44} = 128 ± 2 GPa.

4. DISCUSSION

Considering that the maximum elastic anisotropy and magnetostrictive capability of the Fe-Ga alloys is achieved in a single crystal, a high degree of crystallographic texture of polycrystalline forms is desired to maximize their utility in novel structural and active magnetostrictive components. For example, $Fe_{83}Ga_{17}$ single crystals possess their maximum magnetostrictions in the [100] direction; thus, a polycrystal with a large [100] texture component is desirable. Deformation processing techniques such as rolling may be a promising method to develop a large [100] texture component in Fe-Ga alloys. The well established deformation processing methods for transformer steels (Fe-Si) to realize cubic {100}<001> and the Goss {110}<100> textures and the similarity of Fe-Al alloys system to Fe-Ga alloys makes comparisons of their active slip systems and τ_{CRSS} instructive.

At room temperature, the slip system of the $Fe_{83}Ga_{17}$ single crystals observed in this study are consistent with those of Fe, Fe-Si and Fe-Al alloy systems. $Fe_{83}Ga_{17}$ single crystals exhibited primary slip on the {110}<111> with τ_{CRSS} = 220 MPa (measured in the [110] crystal) and secondary slip on the {211}<111> with τ_{CRSS} = 240 MPa (measured in the [100] crystal). The primary slip system in high purity (99.96%) α-Fe is {110}<111> with τ_{CRSS} = 27.5 MPa and secondary slip occurring on the {211}<111> and {321}<111>. The primary slip system of $Fe_{97}Si_3$ alloy is mixed with {100}<111> and {211}<111> both active at τ_{CRSS} ~ 150 MPa.[12] The aluminides such as $Fe_{60}Al_{40}$ and $Fe_{57}Al_{43}$ single crystals both exhibit primary slip on the {110}<111> with τ_{CRSS} values between 82 and 94 MPa.[13] Notably, τ_{CRSS} is significantly larger for the Fe-Ga and Fe-Al alloys compared to pure α-Fe. According to the Friedel relationships, the increase in τ_{CRSS} with the presence substitutional atoms is due to crystal lattice strain, which provides a larger energy barrier to dislocation movement.[14] The atomic radius of Si, Al and Ga are roughly 10% greater than that of Fe for a coordination number of 8 in the BCC lattice. The stress-strain curves of Fig. 3 and Fig. 5 demonstrate that strain hardening is not evident in either the [100] or [110] samples. This absence of strain hardening indicates a lack of dislocation tie-up and is consistent with the predominance of one active slip system.

Environmental embrittlement may be a factor in the limited elongations of the $Fe_{83}Ga_{17}$ single crystals. The crystal with a tensile axis orientation of [110] began to experience a stress decline beyond 1.3% elongation (Fig. 3), indicating that elongation greater than 1.6% was limited. The crystal with a tensile axis orientation of [100] was pulled to failure with fracture occurring shortly after 2% elongation (Fig. 5). Previous work at room temperature has shown that $Fe_{60}Al_{40}$ and $Fe_{57}Al_{43}$ single crystals both had higher elongations of ~40% before fracture in a dry oxygen atmosphere compared to 20 to 30% in a vacuum and only 10% in air [13]. This embrittlement effect in aluminides is attributed to the catalyzed decomposition of atmospheric water vapor at the metal surface to form hydrogen, which penetrates the material and facilitates crack propagation. Strain rate is also known to be a factor where the elongation of $Fe_{60}Al_{40}$ single crystals in air have been shown to have 6% and 24% elongations respectively for 10^{-6} s^{-1} and 1 s^{-1} strain rates.[15] It is possible that the plastic properties of the FeGa alloys are affected in a similar fashion.

We have observed that the elastic response of α-Fe single crystal was dramatically affected by the addition of Ga. Significant property changes include Young's modulus, Poisson's ratio and the elastic anisotropy. Table 5 summarizes the elastic response for single crystal high purity (99.96%) α-Fe and Fe with up to 27.2 at% Ga. Comparing $Fe_{72.8}Ga_{27.2}$ to pure Fe, the Ga addition caused a large 57% increase in c_{12} while c_{44} increased only 15% and c_{11} declined by 3%. The combined effect of these changes was to reduce $E_{[100]}$ to less than one-sixth of its original value (from 131 to 20 GPa) and raise the elastic anisotropy over eight-fold from 2.4 to 19.9. Accompanying the large increase in elastic anisotropy, the Poisson's ratio for [110] crystal loading became significantly more negative in the $[1\bar{1}0]$ direction with $\nu_{[1\bar{1}0]}$ changing from -0.06 to an extreme value of -0.75.

Table 5. Elastic properties of (99.96%) α-Fe and $Fe_{83}Ga_{17}$. Subscripts indicate the directionality of the property. [A]Data from Mclean *et al.*[6] [B]Data from quasi-static measurements in this study. [C]Data from acoustic measurements by Clark *et al.*[16]

at. % Ga in Fe	in GPa							[100] loading	[110] loading	
	c_{11}	c_{12}	c_{44}	$E_{[100]}$	$E_{[110]}$	$E_{[111]}$	A	$\nu_{[010]}$	$\nu_{[1\bar{1}0]}$	$\nu_{[001]}$
0[A]	228	132	117	131	219	283	2.4	0.37	-0.06	0.61
17.0[B]	225	181	128	65	160	315	5.7	0.45	-0.37	1.11
18.7[C]	196	156	123.1	57	145	297	6.2	0.44	-0.41	1.13
24.1[C]	186	168	120	27	86	293	12.9	0.47	-0.64	1.48
27.2[C]	221	207	135	20	68	334	19.9	0.48	-0.75	1.64

The elastic constants of single crystal $Fe_{100-x}Ga_x$, where $0 \le x \le 27.2$ from Table 5 are used in Eqs. 5 and 6 to examine changes in $\nu_{[1\bar{1}0]}$ and $\nu_{[001]}$ for a [110] loading condition. A plot of these results (Fig. 7) shows a trend of increasingly negative $\nu_{[1\bar{1}0]}$ (from -0.06 to -0.75) and increasingly positive $\nu_{[001]}$ (from 0.61 to 1.64) occurring with increasing Ga content. The elastic anisotropy reflects this trend as A increases from 2.4 to 19.9. The values of $A = 19.9$ calculated for the $Fe_{83}Ga_{27.2}$ alloy is presently the largest anisotropy value known to us. Previous surveys of FCC and BCC metals by Jain *et al.*[8] and Baughman *et al.*[17] report the largest value of $A = 9.2$ for Li. In the case of Li, $\nu_{[1\bar{1}0]} = -0.55$ and $\nu_{[001]} = 1.30$. The Fe-Al alloy system bears similarity to the Fe-Ga alloy studied in this work and suggests that a peak in the elastic anisotropy may occur. For $Fe_{100-x}Al_x$, where $0 \le x \le 40.1$, calculations show an increase from $A = 2.4$ in pure Fe to a maximum $A = 6.5$ occurring for 25.1% Al. The associated Poisson's ratios at this peak anisotropy are $\nu_{[1\bar{1}0]} = -0.44$ and $\nu_{[001]} = 1.10$. Thereafter, A decreases to 3.8 for the 40.1% Al substitution level. Although the level of Ga substitution giving a maximum A remains to be determined, the corresponding minimum $\nu_{[1\bar{1}0]}$ and maximum $\nu_{[001]}$ must be greater than -1 and less than 2, respectively. For example, see the electron-gas model proposed by Baughman *et al.* for the thermodynamically admissible Poisson's ratios.[17] If the quadratic fits of the data in Fig. 6 continue to hold beyond 27.2% Ga, the minimum $\nu_{[1\bar{1}0]}$ and maximum $\nu_{[001]}$ should occur at less than ~32% Ga.

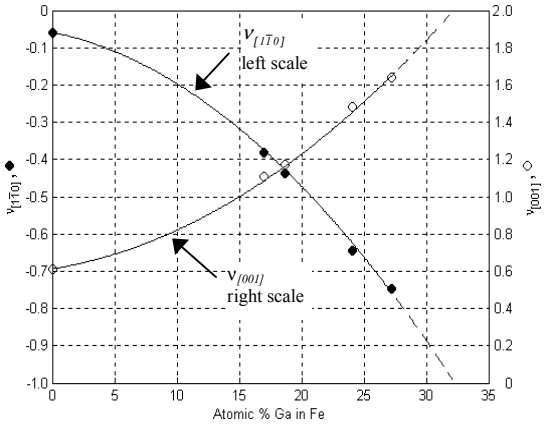

Fig. 7. Calculated Poisson's ratios for [110] loading of $Fe_{100-x}Ga_x$, where x = 0, 17.0, 18.7, 24.1 and 27.2. $\nu_{[1\bar{1}0]}$ and $\nu_{[001]}$ are orthogonal directions which lie respectively in the (001) and $(1\bar{1}0)$ planes. The 17.0% Ga data point was measured in this study while the remaining values are calculated from Eq.5 and 6 using data in Table 5.

5. CONCLUSIONS

Single crystal specimens of Fe-17 at. % Ga were tested in tension at room temperature. These tests indicated that:

- The tensile specimens with a [110] tensile axis orientation elongated at least 1.6%, and slip lines on the specimen surfaces indicated that the active slip plane is the {110}. If the slip direction is assumed to be the <111>, the critical resolved shear stress for {110}<111> slip is 220 MPa. Yielding began at 0.3% elongation and 450 MPa. The ultimate tensile strength was 580 MPa.
- The tensile specimens with a [100] tensile axis orientation elongated at least 2%, and slip lines on the specimen surfaces indicated that the active slip plane is the {211}. If the slip direction is assumed to be the <111>, the critical resolved shear stress for {211}<111> slip is 240 MPa. Discontinuous yielding began at 0.8%

elongation and 515 MPa and may be due to twinning, kink band formation, or stress-induced transformation to another phase.

- The Young's modulus was 160 GPa for loading in the [110] crystal direction with Poisson's ratio of -0.37 on the (001) major face. The Young's modulus was 65 GPa for loading in the [100] crystal direction with Poisson's ratio of 0.45 on the (001) major face. The corresponding elastic constants are c_{11} = 225 ± 20 GPa, c_{12} = 181 ± 20 GPa and c_{44} = 128 ± 2 GPa with an elastic anisotropy of 5.7.
- An Elastic anisotropy value of 19.9 was identified for $Fe_{72.8}Ga_{27.2}$ as well as an in-plane negative Poisson's ratio of -0.75.

These results identifying the active slip systems and shear stresses provide insight to the possible development of texture, or preferred crystallographic orientation, in polycrystalline forms of the Fe-Ga alloys. The common slip mechanisms recognized for the Fe-Ga, Fe-Si and Fe-Al alloy systems suggest that successful texturing methods used for Fe-Si and Fe-Al might be mimicked to optimize polycrystalline Fe-Ga texture for magnetostriction and structural applications. Environmental embrittlement and strain rate dependencies have been observed in Fe-Al and could also be a significant factor for the Fe-Ga alloys. These effects warrant investigation as they affect the strength and formability of the material. The elastic properties of the Fe-Ga alloy were observed to be increasingly anisotropic with rising Ga content for the stoichiometries examined. The large elastic anisotropies generate a remarkably large magnitude negative Poisson's ratio. This negative Poisson's ratio creates a significant in-plane auxetic behavior that could be exploited in applications that capitalize on unique area effects produced under uniaxial loading.

ACKNOWLEDGMENTS

This work was supported by the U.S. Office of Naval Research, the Carderock Division of the Naval Surface Warfare Center and the Office of Basic Energy Sciences, Materials Sciences Division of the U.S. Department of Energy. The assistance of the Ames Laboratory staff and use of their facilities for some of the work reported here is gratefully acknowledged. The Ames Laboratory is operated by Iowa State University for the United States Department of Energy under contract W-7405-ENG-82.

REFERENCES

[1] A. E. Clark, J. B. Restorff, M. Wun-Fogle, T. A. Lograsso, and D. L. Schlagel, IEEE Trans. Magn. **36**, 3238(2000).
[2] J. R. Cullen, A. E. Clark, M. Wun-Fogle, J. B. Restorff, and T. A. Lograsso, J. Magn. Magn. Mat. **226**, 948(2001).
[3] R. A. Kellogg, A. B. Flatau, A. E. Clark, M. Wun-Fogle, and T. A. Lograsso, J. Appl. Phys. **91**, 7821(2002).
[4] A. E. Clark, J. B. Restorff, M. Wun-Fogle, and T. A. Lograsso, Materials Transactions (Japan) **43**, 881(2002).
[5] G.E. Dieter, *Mechanical Metallurgy: SI Metric Edition*, (McGraw-Hill, London, 1988), p. 126.
[6] K.O. Mclean, and C. S. Smith, J. Phys. Chem. Solids (USA) **33**, 279(1972).
[7] J. F. Nye, *Physical Properties of Crystals*, (Clarendon, Oxford,1985).
[8] W. P. Mason, *Physical Acoustics and the Properties of Solids*, D. Van Nostrand (Princeton, New Jersey 1958), A1.
[9] M. Jain, and M. P. Verma, Indian J. Pure Appl. Phys. **28,** 178(1990).
[10] F. Milstein, and K. Huang, Phys. Rev. B **19**, 2030(1979).
[11] J. J. Cox, R.F. Mehl, and G.T. Horne, Trans. Am. Soc. Met. **49**, 118(1957).
[12] B. Orlans-Joliet, J.H. Driver, F. Montheillet, Acta Metallurgica **38**, 581(1990).
[13] I. Baker, D. Wu, E.P. George, Structural Intermetallics, p. 279,(2001).
[14] F. Nabarro, Proc. R. Soc. (London) A **381**, 285(1982).
[15] D. Wu, I. Baker, Intermetallics **9**, 57(2001).
[16] A. E. Clark, J. B. Restorff, M. Wun-Fogle, and T. A. Lograsso, accepted for publication, J. Appl. Phys., June (2003).
[17] R. H. Baughman, J.M. Shacklette, A. A. Zakhidov, and S. Stafstrom, Letters to Nat. **392**, 362(1998).